Engineering and Technology Journal

The Effect of Rectangular Grooves on the Lubrication Mechanism in an Inclined Slider Bearing

Muhannad M. Mrah[*], Ammar S. Hamid Merza [ID]

Mechanical Engineering Dept., University of Technology-Iraq, Alsina'a street, 10066 Baghdad, Iraq.
*Corresponding author Email: me.19.23@grad.uotechnology.edu.iq

HIGHLIGHTS

- The pressure distribution increased at 3mm groove width compared to 5mm and 8mm.
- The grooved models are lower than 0.5, 4.2, and 14.6% of the load capacity of the flat model.
- The flat model coefficient of friction is lower than the grooved models by 0.3, 4.6, and 17.3%.
- The maximum load-carrying of flat and grooved models was in the film ratio (K) = 2–2.5.

ARTICLE INFO

ABSTRACT

This research aims to study the effect of rectangular grooves on the lubrication mechanism in an inclined slider bearing. Reynolds' equation was used in the theory part to calculate the pressure gradient in a one-dimensional fluid film. The tilted sliding bearing compared the practical results, where the researcher manufactured and developed the device by adding pressure sensors along with the pad. These sensors will give accurate readings because they will read the pressure directly from the bottom of the pads without manometer tubes. Four pads were manufactured, one without grooves and three with rectangular grooves, varying slot widths (3, 5, 8 mm), and a depth of 2mm. This study examined various variables: sliding velocities, pad inclination values, and oil temperatures. The conclusions indicated that the flat model is significantly superior to the groove's models. One significant finding for grooved models is that as the inclination increases, the maximum load capacity approaches the pad's center, allowing grooved models to be used in applications requiring less load and weight. The maximum load-carrying capacity of flat and grooved models was in the film ratio (K) = 2–2.5. In contrast, the load capacity of the flat model was greater than that of the groove model by percentages of 0.5%, 4.27%, and 14.66%, respectively. Moreover, the flat model's coefficient of friction is lower than the coefficient of friction of the groove models, with percentages of 0.38%, 4.63%, and 17.37%, respectively.

1. Introduction

1.1 General

The movement of contact surfaces varies from macro to micro scales, from continental plates and glaciers to animal and insect locomotion. It is controlled by surface topographies, lubricant layers, contaminants, operating conditions, and others, i.e., this motion depends on a system's tribological characteristics. Before the industrial revolution, the application of animal fat or oil-controlled friction and wear. With the advent of trains and other equipment, operating conditions on touch surfaces improved significantly after the industrial revolution. Understanding the lubrication pathways involved has been significant. The field of tribology has acquired considerable popularity, i.e., it has become apparent that technological advancement will be limited without developments in tribology [1].

The development in various fields of mechanical technology and the competition of production companies to produce mechanical parts that work with high efficiency and performance and save energy from loss have made the science of friction, corrosion, and lubrication, i.e., tribology, a center of attention and research and development.

Recently, surface texturing has been used to improve the tribological characteristics of mechanical components. Texturing a surface can be advantageous in various ways; for example, it can reduce friction and wear, increase load-carrying capacity, and increase fluid film stiffness [2-4]. Generally, the primary functions of surface texturing are to act as traps for wear debris [5], to control adhesion and stiction [6], to provide reservoirs for improved lubricant retention [7], and to generate hydrodynamic pressure to increase load-carrying capacity [8,9], among others. With these capabilities, it is not surprising that surface texturing is widely used in various fields, including thrust bearings [10-12] and journal bearings [13].

218

1.2 Thrust Bearings

Thrust bearings are generally designed to transfer high axial loads from the rotating shaft. These bearings are widely used in rotating machines such as turbines, compressors, pumps, etc., because of their low friction, good load-bearing, and high damping characteristics. The surface above the pads has a significant impact on the bearing life. Thus, previous literature indicates [2-4] that surface texturing profiles significantly influence the load-carrying capacity of bearings. Over the last few years, considerable research has focused on enhancing the performance of these bearings. The latest bearings were developed by A. G. M. Michell in Australia and A. Kingsbury in the USA [14]. Given the significance of these parts for rotating machines, much research has been dedicated to evaluating their behavior and investigating the different factors that affect their correct functioning (maximum pressure, load-carrying capacity, and power loss).

On pivots, the bearing has sectional shoes or pads, As shown in Figure 1. When the bearing runs, the spinning portion transports new oil into the pad region via viscous drag. Due to the fluid pressure, the pad tilts slightly, generating a slight constriction between the shoe and the opposite bearing surface. The pad's tilt adjusts adaptively in response to bearing load and speed. Numerous design features guarantee that the oil is replenished continuously, preventing overheating and pad damage.
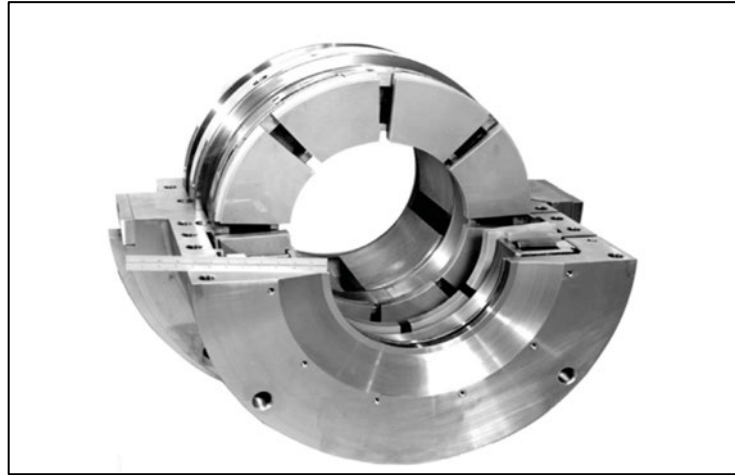
Figure 1: Thrust Bearing [15]

Michell/Kingsbury fluid bearings find application in a broader range of heavy-duty rotating machinery. This is because they are more compact, less expensive, need less maintenance, last longer, and are more effective. Despite this, the oil film's added benefits in stress absorption enabled damping to be used as a design parameter [16]. For example, hydroelectric facilities sustain turbines and generators weighing hundreds of tonnes [17]. Additionally, they are utilized in huge machinery, such as dynamic towers, due to their load capacity, longevity, and stability during operation [15].

1.3 Objectives

The previous scientific literature that discusses the combined effects of pad surface profile assumes flat pads with no rectangular slots in the surfaces. However, the goal of reducing friction and the desire to get the highest load capacity in the operating conditions of tilting-pad thrust bearings resulted in the following research question: The wide applications of sliding bearings in mechanical devices give great importance to the study of their design. Is it possible to achieve performance improvements, i.e., a lower friction coefficient and higher load-carrying capacity, by applying features like rectangular grooves to the surfaces of the bearing pads?

The design of sliding bearings is subject to many considerations. Usually, bearing designers try to select design variables within constraints through trial and error methods, using design schemes resulting from the analysis of bearing characteristics. Unfortunately, this method often produces unconvincing results and does not give the optimal design solution. Thus, the optimal design of sliding bearing shapes has become an essential and exciting topic in recent years.

In this research, it is essential to obtain the optimal design of inclined bearings that meets the desired ambition of obtaining the highest load capacity and the lowest friction and, thus, obtaining the lowest energy consumption in the machine during lubrication.

2. Experimental Work

The plane slider bearing is probably the most tractable use of Reynolds' equation for the pressure gradient in a fluid film. Practical implementations are varied and significant, of which the Michell tilting pad slider bearing is the most common [18]. The apparatus used in this work illustrates some of the critical aspects of a tilting pad and slider bearing.

2.1 Experimental Apparatus

The system consists of a plane aluminum slider, 12.5cm²; Dimensions are placed precisely in proportion to the movable belt, which carries a thick oil film. Figure 2. shows a diagram of the device used, consisting of two rotating cylinders (A, B) connected by an oil conveyor belt. The cylinder (A) is driven by an electric motor through which the cylinder rotation speed can be controlled and thus the linear velocity of the conveyor belt. Models with the exact dimensions as the slider but a

thickness of 4mm can be installed in the lower area of the slider. It contains pressure gauge holes attached to it and plastic tubes that transfer the oil pressure to the sensors to measure the oil pressure inside the sample, and these tubes are longitudinally distributed. To calculate the change in pressure resulting from the trapping of oil between the moving belt and the model tilted at a certain angle and cross tubes to indicate the balance and level of the device, the oil flows from (C) to region (D). The clearance between the belt and the sample is controlled by a micrometer at the edge (C, D), and the device is placed in a basin, part of which is filled with oil.
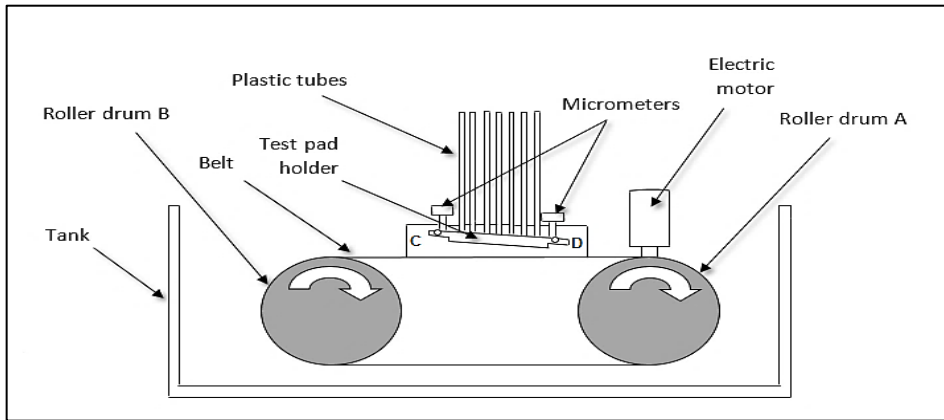

Figure 2: Schematic of the experimental apparatus

Two micrometers determine the clearance between the slider and the belt. They are positioned parallel to the leading and trailing edges of the slider. One of these micrometers was fixed to the lead edge, while the other was fixed to the trailing edge. Thirteen sensors attached to the slider indicate the amount of oil pressure created by the slider and the moving belt via plastic tubes. Seven of these sensors are evenly spaced along the slider's axis in the direction of movement. At the same time, another group is transversely located in a plane roughly parallel to the point where the oil's maximum pressure is supposed to occur [18]. The device used with the additional instruments is depicted in Figure 3.
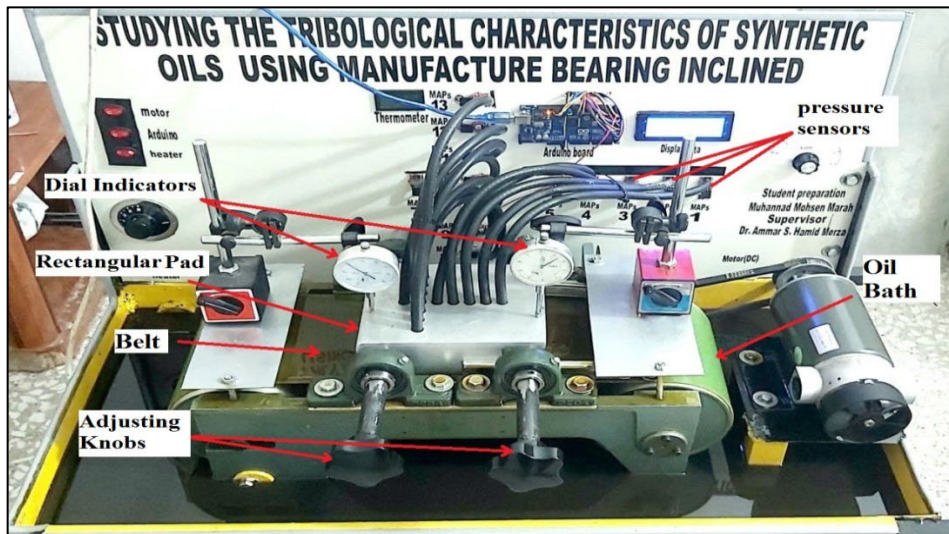

Figure 3: The tilting-pad bearing test rig

2.2 Experimental Models

Aluminum was used as the metal for the produced models; the thickness of the manufactured models is 4mm. This metal was chosen for its availability and simplicity of installation on the equipment. The metal was chopped into squares (12.5 cm²) to match the models (4). A CNC machine was used to create rectangular grooves on the models. Four pads were manufactured, one without slots and three with rectangular grooves (orienting the grooves in the direction of the oil flow) and varying slot widths (3, 5, and 8 mm), and a depth of 2mm, as shown in Figure 4a. The models must be identical in size to the holes in the equipment used, have the same diameter, and have the same number of holes (13), as shown in Figure 4b. These holes are placed next to the pad's holes to allow oil to flow through the pipes to measure the oil pressure.
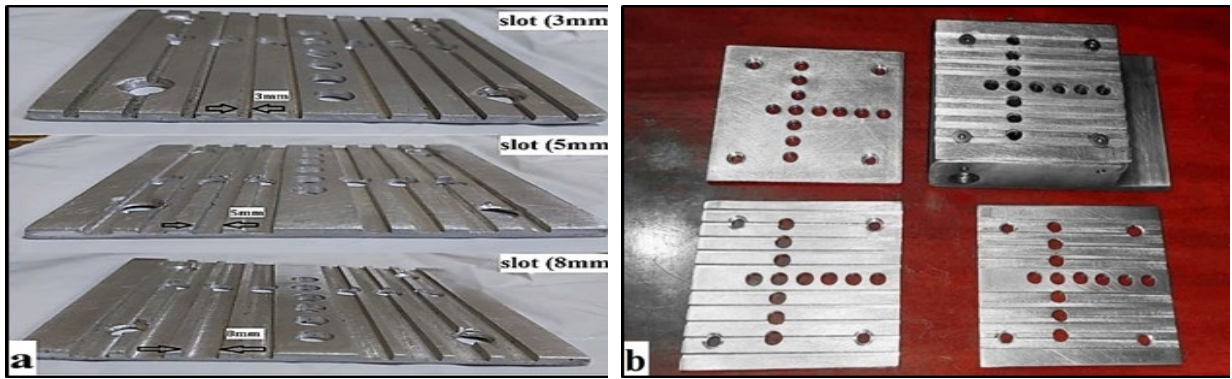
Figure 4: The pad models: a. the width of the slots, b. the distribution of the holes on the pads

2.3 The Test Procedure

1. A model was chosen for testing.
2. The model was connected to the device.

Connection requirements: Opening the upper portion of the device requires dismantling the eccentric shafts and sliding pad to connect the model to the device's sliding pad surface. When a connection is made, the model must be placed on the pad of the original machine, with the model's holes (13 holes) aligned with the holes of the original machine, using the four flat head screws between the model and the pad of the actual device, and then the device's upper part must be reconnected.

3. Fill the basin with oil submerged in the bottom portion of the belt, at least partly filling the basin with 10 liters.
4. The entrance-to-exit film thickness ratio was adjusted to the appropriate value on both micrometers.
5. The operation of the devices was as follows:
   • Heater was run at the required degree for heating.
   • Running the DC drive to rotate the belt (which helps to distribute the oil temperature in the basin).
6. The motor was driven for many minutes until the steady start condition was achieved, at which point the oil in each pressure sensor reached a consistent value.
7. At each sensor, the pressure value was measured and recorded.
8. Repeat the preceding procedures for a four-speed sliding.
9. Repeat the preceding procedures to alter the four values for (K) until all tests per model are completed.
10. A different model was selected, and the identical procedures as above were followed. Figure 5 illustrates the fundamental stages of testing.
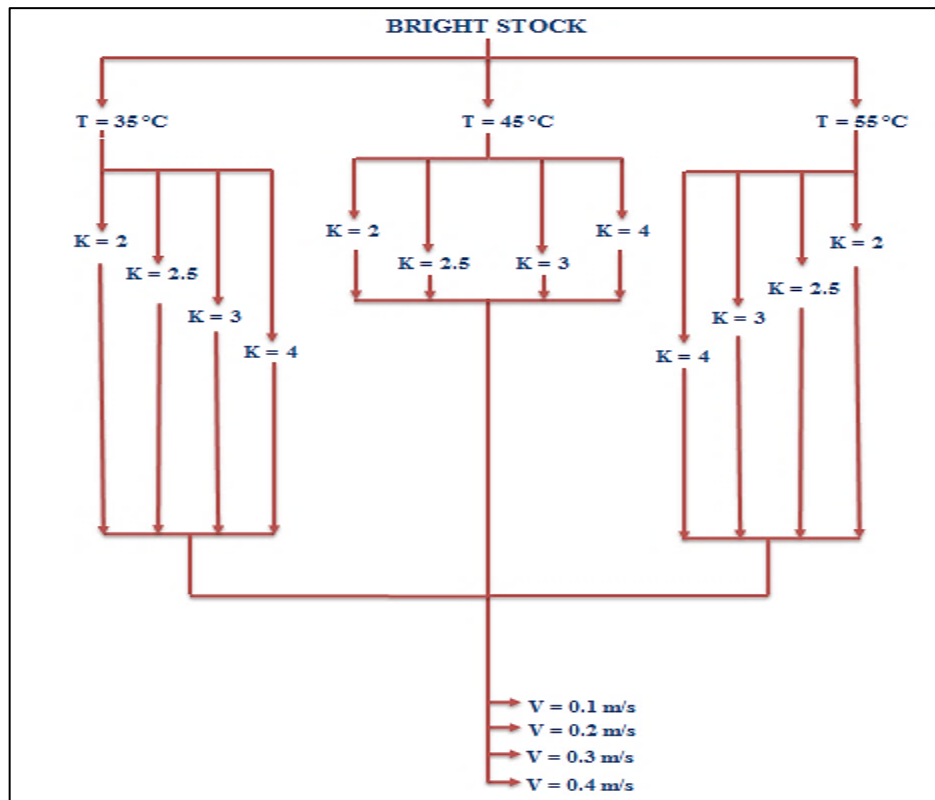

Figure 5: Test procedure for models

3. Fundamental Theoretical Considerations

The Reynolds equation describes the change of lubricating pressure in a bearing. The inclined plane pad is the most popular lubricated slider bearing, which demonstrates how the Reynolds equation may be used for slider bearings (where this type has been studied in this research). The complete equation is complicated to solve. Still, a reduced form will be utilized in the first instance by making several derivational assumptions and using the equilibrium of a tiny element to derive the Reynolds equation in one dimension [18].

3.1 Assumptions

We make the following assumptions:

1) Body forces are disregarded, which implies that no external force field, such as gravitational or magnetic forces, acts on the lubricant [19].
2) The fluid is incompressible and Newtonian (obeying Newton's law of viscosity) [20].
3) The flow is laminar.
4) The bearing is infinitely vast.
5) The viscosity of the film remains constant throughout its thickness. This is undoubtedly not true, but it adds a layer of complication if not accepted [20].

3.2 Reynolds' Equation Applied to Sliding Bearings

The following equation was developed to express the change in pressure along a converging fluid film in terms of the velocity gradient across the film [18]:

$$\frac{dP}{dx} = \eta \frac{d^2u}{dy^2} \tag{1}$$

$$\text{or} \quad \frac{d^2u}{dy^2} = \frac{1}{\eta}\frac{dP}{dx} \tag{2}$$

Integrating Eq. (2) twice with respect to y gives:

$$u = \int \frac{1}{\eta}\frac{dP}{dx}y \, dy + C_1 \, dy = \frac{1}{2\eta}\frac{dP}{dx}y^2 + C_1 y + C_2 \tag{3}$$

In Figure 6. The constants of integration C_1 and C_2 may be evaluated from the boundary conditions:

1) $u = U$ when $y = 0$
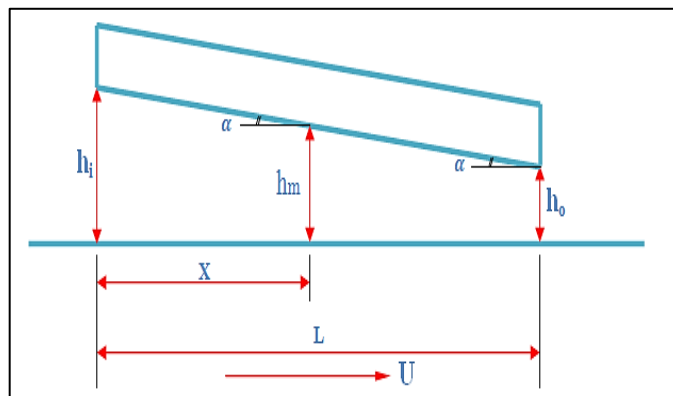2) $u = 0$ when $y = h$

Figure 6: Geometry of a linear pad bearing

From condition (1), it follows that $C_2 = U$ and from condition (2)

$$C_1 = -\frac{1}{2\eta}\frac{dP}{dx}h - \frac{U}{h}$$

By introducing the values of these constants into Eq. (3), it becomes:

$$u = \frac{1}{2\eta}\frac{dP}{dx}(y^2 - hy) + U\frac{h-y}{h} \tag{4}$$

The first component in the right-hand member of Eq. (4) denotes a parabolic velocity distribution caused by the film's pressure-driven flow. The second component in Eq. (4)'s right-hand member illustrates a linear velocity distribution caused by

the two surfaces' relative motion. Now we need to find an expression for the volume of fluid flowing through the bearing. By using the above assumptions and defining (Q) as the volume of fluid flowing in a unit of time,

$$Q = \int_0^h u \, dy$$

By substituting the value of u from Eq. (4) and integrating, the equation for (Q) becomes,

$$Q = \frac{Uh}{2} - \frac{h^3}{12\eta} \frac{dP}{dx}$$

For an incompressible fluid, the flow is the same for all cross-sections of the film, or

$$\frac{dQ}{dx} = 0$$

Therefore,

$$\frac{dQ}{dx} = \frac{U}{2} \frac{dh}{dx} - \frac{d}{dx}\left(\frac{h^3}{12\eta} \frac{dP}{dx}\right) = 0$$

$$\frac{d}{dx}\left(h^3 \frac{dP}{dx}\right) = 6 \, \eta \, U \, \frac{dh}{dx} \tag{5}$$

This is the one-dimensional Reynolds equation for the pressure gradient in a converging fluid film, which is ignored by side leakage (flow in the z-direction).

Note: This general formula is used exclusively for theoretical and experimental comparisons of flat pads. In the case of grooved pads, only experimental results are discussed.

3.2.1 Pressure and load capacity distributions

Integrating Eq. (5) twice with respect to **X** gives:

$$P = \frac{6 \, \eta \, U \, L}{h_0^2}\left(\frac{K-1}{K+1} \frac{\frac{X}{L}(1-\frac{X}{L})}{[K-(K-1)\frac{X}{L}]^2}\right) \tag{6}$$

Further integration of Eq. (6) yields the sliding bearing's normal load capacity per unit width:

$$\frac{W}{B} = \int_{x=0}^{x=L} P \, dx \tag{7}$$

The load-bearing capacity equation becomes:

$$W = \frac{6 \, \eta \, U \, L^2 \, B}{h_0^2} \frac{1}{(K-1)^2}\left(\log_e K - \frac{2(K-1)}{K+1}\right) \tag{8}$$

3.2.2 Shear stress in the hydrodynamic film

To evaluate the shear stress along the length of the bearing at the lower surface, the definition of Newtonian viscosity and Eq. (4) is used to get:

$$\tau_o = -\frac{h}{2} \frac{dP}{dx} - \frac{\eta U}{h} \tag{9}$$

Also, the shear stress at the upper surface:

$$\tau_h = \frac{h}{2} \frac{dP}{dx} - \frac{\eta U}{h} \tag{10}$$

3.2.3 Friction force

Friction is the resistance to motion between two solid bodies as one slides over the other. The resistive force perpendicular to the direction of motion is referred to as the "friction force" Even such negligible frictional forces result in energy waste and subsequent loss of machine efficiency. As a result, the designer's goal is often to minimize frictional forces. The frictional force is calculated using the following equation:

$$F = \int_0^L \tau \, dx \tag{11}$$

The friction force on the lower surface is

$$F_o = \frac{\eta\,U\,L\,B}{h_o}\left[\frac{4\log_e K}{K-1} - \frac{6}{K+1}\right] \tag{12}$$

$$F_h = \frac{\eta\,U\,L\,B}{h_o}\left[\frac{2\log_e K}{K-1} - \frac{6}{K+1}\right] \tag{13}$$

3.2.4 Coefficient of friction

As it is known that

$$\mu = \frac{F}{W} \tag{14}$$

Substituting for W and F and simplification the above equation yields:

$$\mu = \frac{h_o}{L}(K-1)\left[\frac{2(K+1)\log_e K - 3(K-1)}{3(K+1)\log_e K - 6(K-1)}\right] \tag{15}$$

3.3 Experimental Calculations

The seven pressure sensors were tested with a constant belt speed for a range of film ratios, with the film thickness h_o at the trailing edge remaining constant. In contrast, the film thickness at the leading edge gradually increased [21]. The following are the corresponding calculations for a few of these tests see Table 1:

Table 1: List of parameters used in experimental calculations

Models	Flat
Type oil	Bright stock
Temperature	35°C
Film ratio K (hi/ho)	2
Pad length (L)	0.125 m
Belt length	1.25 m
Sliding velocity	0.1 m/s
Density	900 kg/m³
Viscosity of oil at T=35°C	395 cSt

Generally, kinematic viscosity is expressed in centistokes. The relationship between viscosity (η) expressed in centistokes and SI units is as follows:

$$\upsilon = (cSt) \times 10^{-6} \qquad m^2/s$$

Given that kinematic viscosity is defined as (viscosity)/(density), the following may be written:

$$\eta = \rho\upsilon = \rho\,(cSt)\,10^{-6} \qquad kg/ms$$

a) The Pressure was calculated using Eq. (6). See Table 2.

$$P = \frac{6\,\eta\,U\,L}{h_o^2}\left(\frac{K-1}{K+1}\frac{\frac{X}{L}(1-\frac{X}{L})}{[K-(K-1)\frac{X}{L}]^2}\right)$$

Table 2: List of simple calculations

station	1	2	3	4	5	6	7
P(practical) pa	230	736	1393	2157	2835	3240	3160
P(theoretical)pa	329	985	1943	2827	3565	4060	4005

Note: The above table makes it possible to calculate the error rate between the theoretical and experimental parts, as the error rate is estimated at about 23%. The presence of such a percentage is due to the natural leakage of oil from both sides of the pad, in addition to the vibrations emanating from the motor, as well as the design of the pad (roughness and texture).

b) The load capacity was calculated by using Eq. (8).

$$W = \frac{6\,\eta\,U\,L^2\,B}{h_o^2}\frac{1}{(K-1)^2}\left(\log_e K - \frac{2(K-1)}{K+1}\right)$$

$$W = \frac{6*0.33*0.1*(0.125)^2*0.125}{(0.0005)^2}\frac{1}{(2-1)^2}\left(\log_e 2 - \frac{2(2-1)}{2+1}\right)$$

$$W = 40.962 \ N$$

c)   The coefficient of friction was calculated by using Eq. (15).

$$\mu = \frac{h_o}{L}(K-1)\left[\frac{2(K+1)\log_e K - 3(K-1)}{3(K+1)\log_e K - 6(K-1)}\right]$$

$$\mu = \frac{0.0005}{0.125}(2-1)\left[\frac{2(2+1)\log_e 2 - 3(2-1)}{3(2+1)\log_e 2 - 6(2-1)}\right]$$

$$\mu = 0.01945$$

4. Results and Discussion

4.1 Effect of Variables on The Pressure Distribution

4.1.1 Sliding speeds affect the mean pressure distribution

Figures (7a-d) explain the experimental results of the connection between the average pressure distribution and the sliding speed of the oil for grooves models compared with the flat model. It is evident from the figures that the pressure is directly proportional to the sliding speed. As the belt speed increases (the speed of the oil slip), the amount of oil trapped between the belt and the cushion increases, increasing the P mean inside the tubes. Thus, an increase in the sensor reading for the flat model. As for the grooved models, they are constructed similarly to the flat model, except that the distance between the belt and the cushion will be greater due to the presence of grooves that require a more significant amount of oil to fill and because the flow is constant, the average pressure of the flat model will be greater than the pressure of the grooved model.
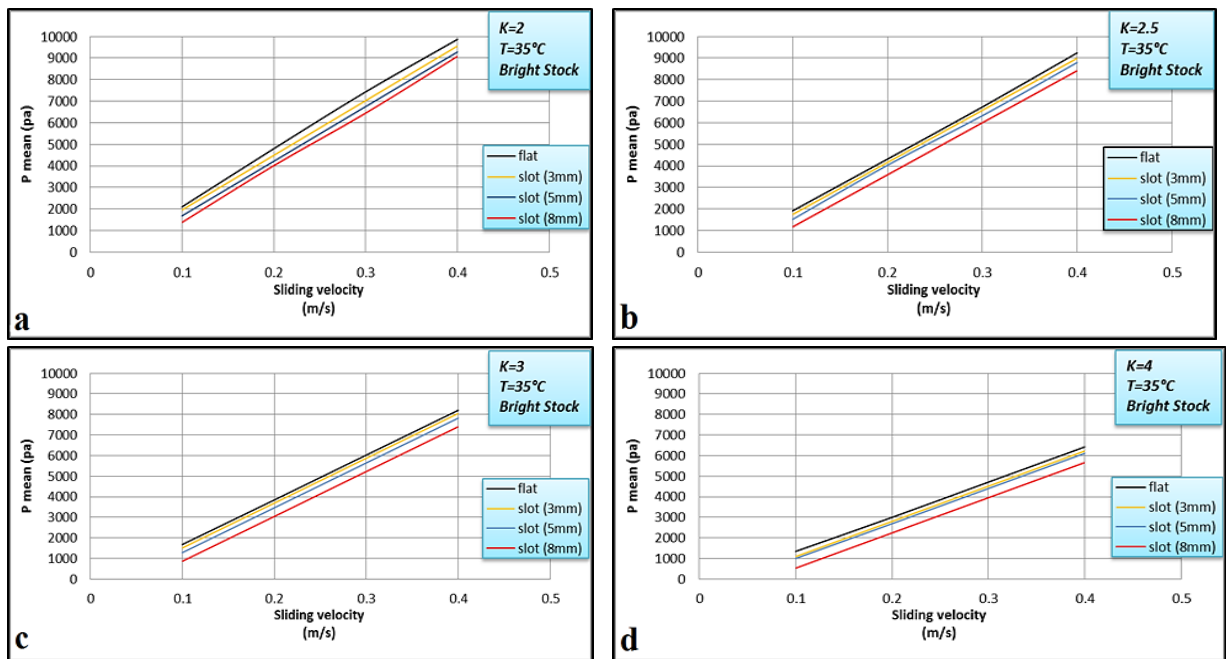
■ P mean (flat plat > slot 3 mm > slot 5 mm > slot 8 mm)

Figure 7: (a-d) Relation between Pmean and sliding velocity at T=35ºC and Various values of K

4.1.2 Effect of temperature on the mean pressure distribution

Figure (8a-d) shows the relationship between oil temperature and average pressure. In general, when the oil temperature increases, the pressure decreases due to the decrease in intermolecular forces as the molecules move away from each other, causing the fluid to expand and thus reduce its viscosity. In this case (constant flow rate), when the oil's viscosity decreases, the oil's adherence to the belt decreases, so the amount of oil trapped between the belt and the pad decreases, and thus the pressure readings in the sensors decrease. In addition, the presence of grooves increases this size (the greater the width of the grooves, the greater the volume) and therefore requires more oil compared to a flat pad, which has the least confined volume, so it gives higher pressures.

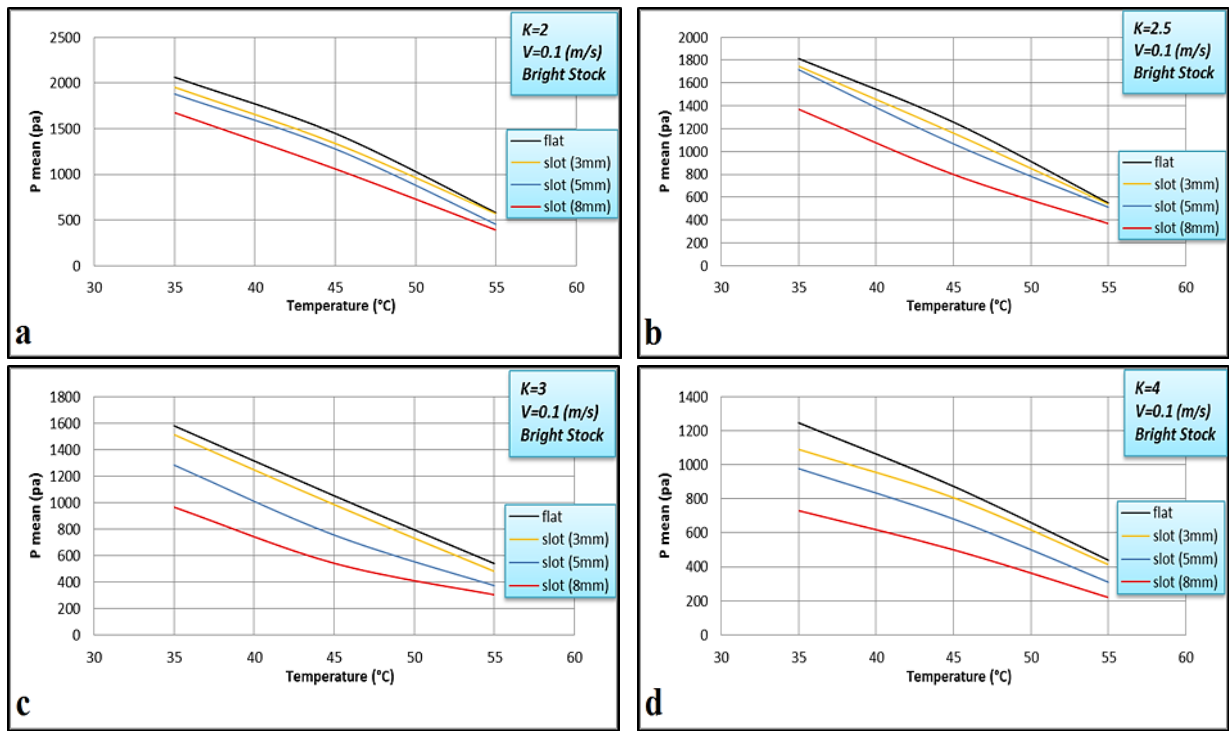■ P mean (flat plat > slot 3mm > slot 5mm > slot 8mm)

Figure 8: (a-d) Relation between Pmean and temperature at V= 0.1 (m/s) at different values of K

4.1.3 Effect of an inclination on the mean pressure distribution

The relationship between the inclination of the pad and the average pressure is depicted in Figure 9. In general, when the pad is parallel to the belt, no hydrodynamic pressure is generated due to the absence of a wedge, which is one of the conditions for generating hydrodynamic pressure [18]. However, when the pillow tilt begins, pressure generation begins, and when the inclination of the pad is (K = 2), the highest hydrodynamic pressure occurs. Then, with the increase in the inclination of the pad, the pressure begins to decrease to increase the volume confined between the pad and the belt. The presence of grooves increases this size and thus reduces pressure compared to a flat pad.
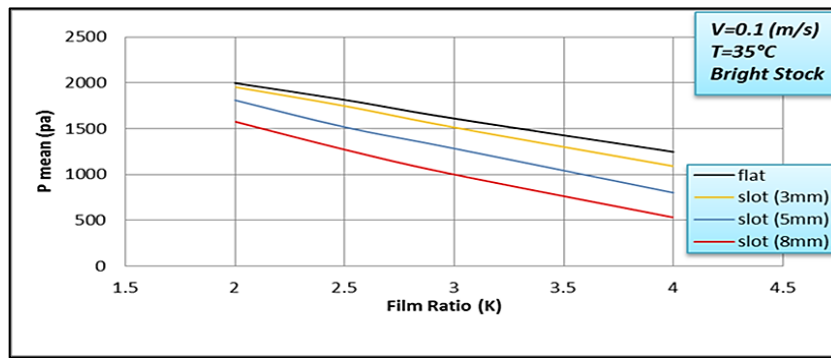

Figure 9: Relation between Pmean and film ratio (K) at V= 0.1 (m/s) and T=35°C

4.2 Effect of Variables on The Load-Carrying Capacity

4.2.1 Sliding speeds effect on the load-carrying capacity

Figure (10a-d) shows the relationship between the load-carrying capacity (W) and sliding velocity of the oil for grooves models compared with the flat model. Where the Pmean increases with sliding velocity increase, The reason for this behavior is the variable [(V) in Eq. (8)] that will affect the values of the load-carrying capacity. So, when the sliding velocity (directly proportional to the load-carrying capacity) has been increased, the P mean (directly proportional to the load-carrying capacity) will also increase. So, for this reason, the load-carrying capacity will increase at various sliding velocities. As we have noted in the previous figures, the average pressure of the flat model is higher than the average pressure in the groove models. Therefore the loading capacity of the flat model is higher than the other models. The load capacity of the flat model was more significant than the load-carrying capacity of the groove models by percentages of 0.5%, 4.27%, and 14.66%, respectively. That is, we conclude that when using large-sized pads (which are more expensive), we can benefit from the presence of grooves with a width of 3mm, which save metal and weight and thus result in a lower cost for all of this while retaining less than 0.5% of the load-bearing capacity compared to a flat pad.
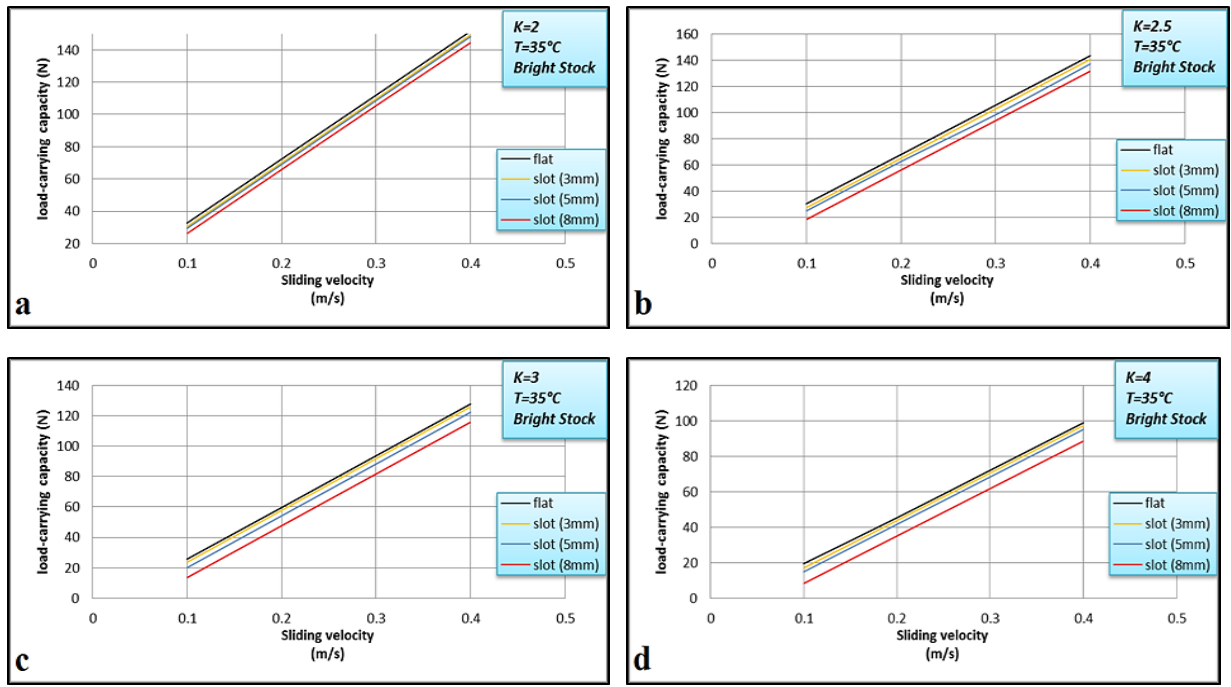
Figure 10: (a-d) Relation between load capacity and sliding velocity at T=35ºC and various values of

4.2.2 Effect of an inclination on the load-carrying capacity

from Figures (11a-c), we can get the effect of temperature on the load capacity and film ratio. We observe that as the inclination increases, the load-carrying capacity decreases (inverse proportion). This is because the higher the inclination value, the more volume is constrained between the pad and the belt. As a result, the oil pressure is reduced (constant flow rate) compared to the flat pad. In the case of grooved pads, the presence of grooves increases the value of K, resulting in a more significant decrease in pressure. When the value of (K) is between (2-2.5), the maximum increase in (W) occurs, and then the value of (W) steadily decreases as the value of (K) increases. This is more accurate than what Gropper et al. recommended in their review (The highest load capacity is obtained whenever the value of the inclination of the pad is close to zero) [22].
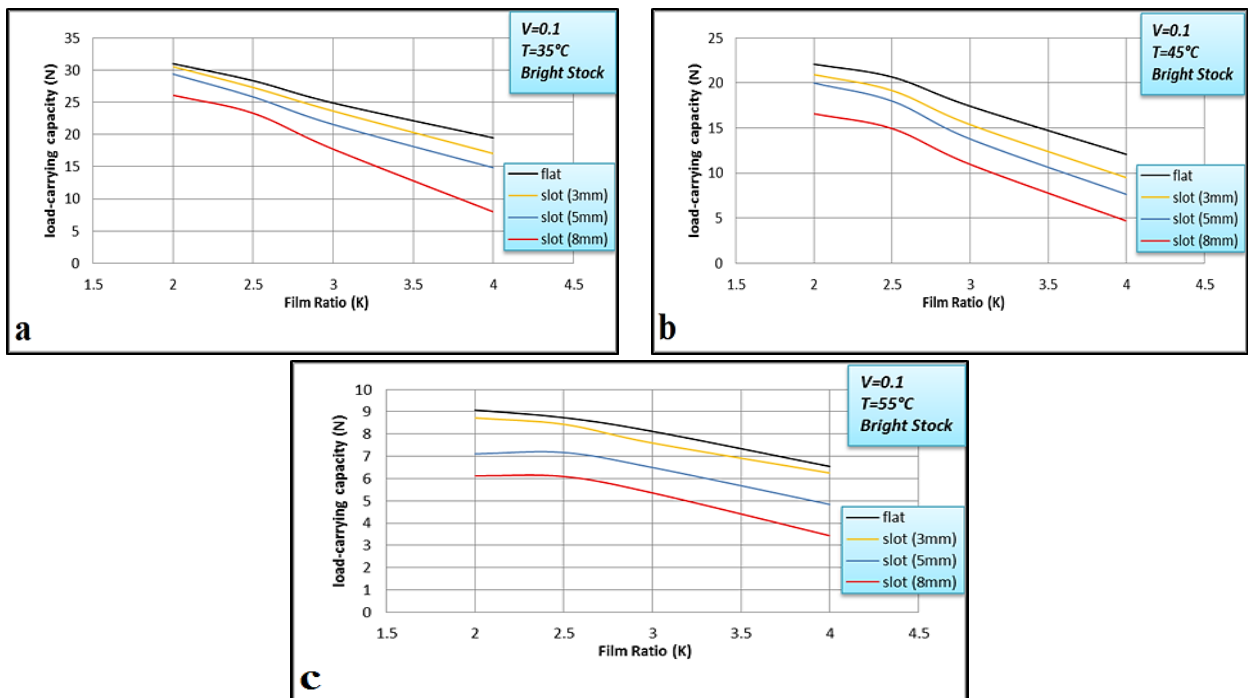

Figure 11: (a-c) Relation between load capacity and film ratio at V= 0.1 at different temperatures

4.3 Effect of Variables on The Coefficient of Friction

4.3.1 Effect of sliding speeds on the coefficient of friction

Figure (12a-d) shows the relationship between slip speed and the coefficient of friction. In general, when the sliding speed increases, the coefficient of friction decreases (an inverse relationship). Since the sliding speed increases, the load-carrying capacity will also increase, which is inversely proportional to the friction coefficient. When the surface is flat, the load capacity will be higher than that of the grooved surfaces, and thus the lowest coefficient of friction will be obtained. Whereas, when the surface is grooved, the load capacity will be less than the flat surface [(W slot 3mm > W slot 5mm > W slot 8mm)], and thus, you will get the highest coefficient of friction (the friction surface area is larger in the presence of grooves). We note that the coefficient of friction for all surfaces is at its maximum when the sliding speed is low, and the reason for this is that the load capacity is very low compared to the friction force between the oil and the belt.

4.4 Pressure Distribution Along The Pad

Figures (13a-d) depict the relationship between the pressure at any location on the pad's surface and the proportion between (X/L) for grooved models and flat ones. The pressure value begins at zero at the pad's leading edge. Then, it steadily grows throughout the pad's length until it reaches its maximum value in the pad's back half (where the fluid adhering to the moving surface will be dragged into the narrowing clearance space, thus building up a pressure sufficient to carry the load). Finally, the pressure value will decline until it hits zero at the pad's trailing edge.
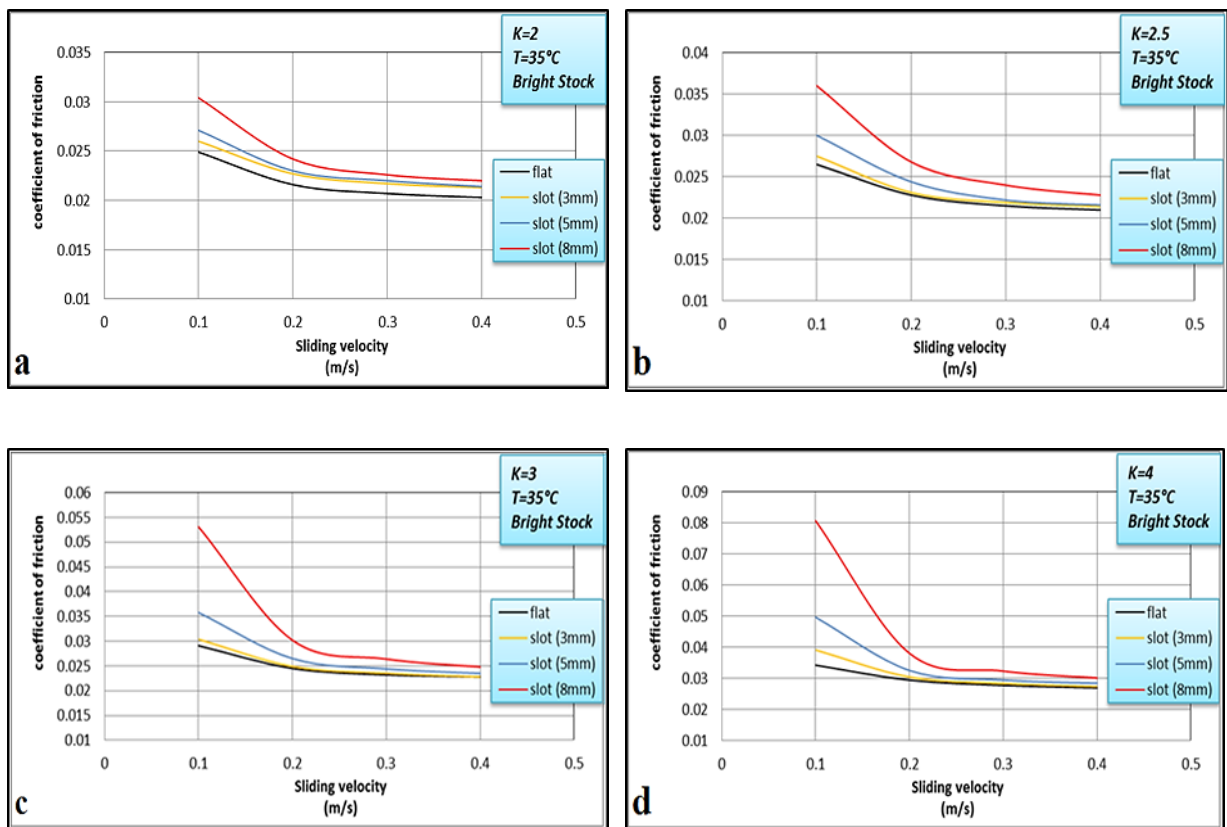

Figure 12: (a-d) Relation between the coefficient of friction and sliding velocity at various values of K

As illustrated in Figures (13c and d), flat pads provide the highest average pressure of the other models. This is because the distance between the pad and the belt is smaller for the flat surface model than for the other models, implying that the confined fluid volume is smaller.

One important point to note is that as the value of K increases, the maximum average pressure of the groove pads begins to approach the center of the pad. This is because the grooves increase the surface friction, which works to return the maximum pressure to the center of the pad approximately.
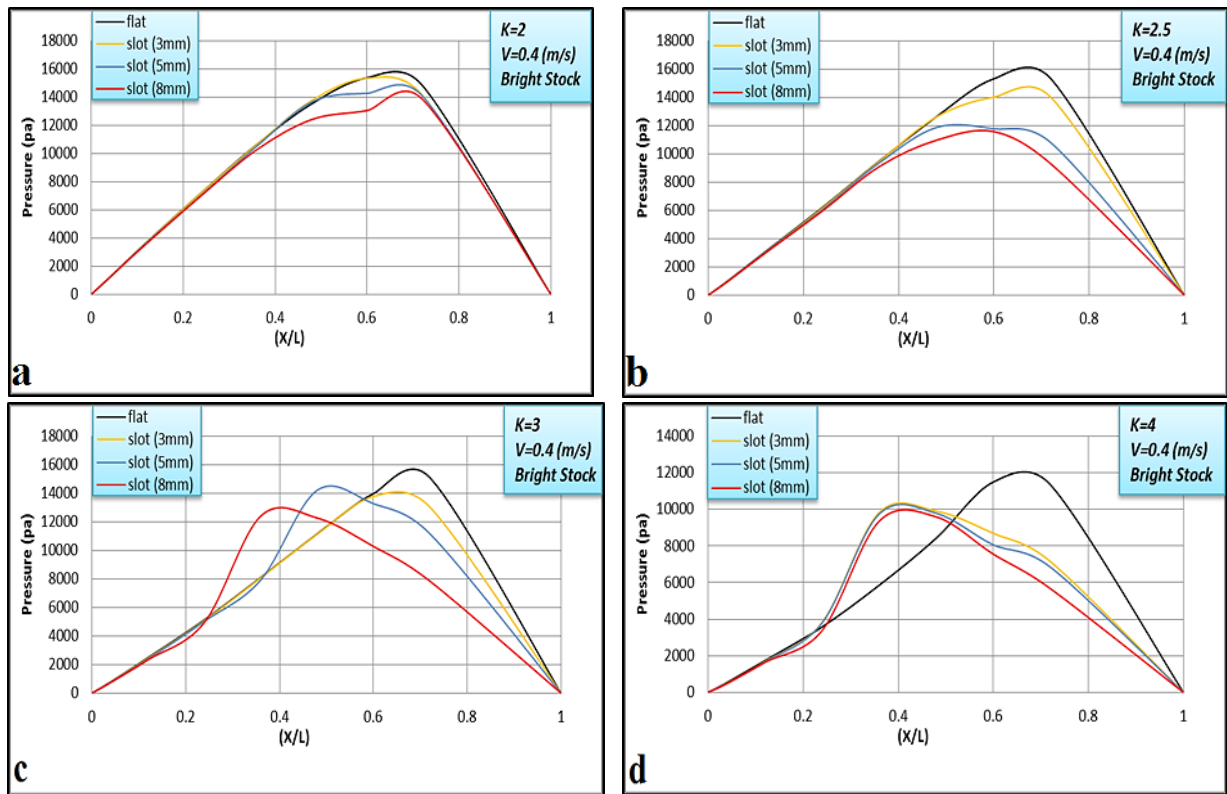
Figure 13: (a-d) Pressure distribution for all models at T=35°C and various values of K

4.5 Comparison Between the Present Work and the Previous Work

The current work was compared to previous work [23]. This comparison used a flat sample. Pressure sensors [24] were used in the current work, whereas manometer tubes were used in the previous work. As illustrated in Figure 14, the pressure distribution at the current work is higher than at the previous work (but with the same behavior). This is because the sensors take direct readings from the bottom of the pad's surface. In previous work, readings were taken by observing the liquid level inside the manometer tubes. The liquid inside the tubes has a different density than the liquid beneath the pad's surface due to the temperature difference between the oil and the surroundings. Since temperature differences affect fluid density, most of the research on the pressure distribution in a sliding inclined bearing should pay close attention to this factor.
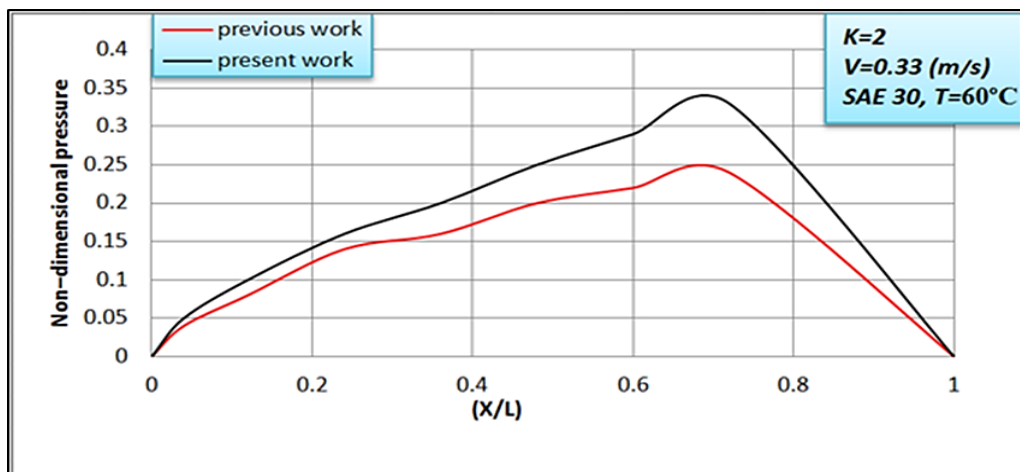

Figure 14: Comparison between the present work and the previous work

5. Conclusions

Based on the experimental analysis of the findings, the following conclusions can be drawn from the present work:

1) When a flat model is used instead of a groove model, the pressure distribution is improved for the same operating circumstances.
2) For grooves models, the pressure distribution has been increased at (groove width of 3mm) more than the increase at (groove width of 5mm and 8mm).

3) The flat model's coefficient of friction is lower than the coefficient of friction of the groove models, with percentages of 0.38%, 4.63%, and 17.37%, respectively.
4) The maximum load-carrying capacity of flat and grooved models was in the film ratio (K) = 2–2.5. In contrast, the load capacity of the flat model was more significant than the load-carrying capacity of the groove models by percentages of 0.5%, 4.27%, and 14.66%, respectively.
5) Pressure distribution improved when the belt speed was raised, irrespective of the test model.
6) One significant conclusion for models with grooves is that as the inclination increases, the maximum load capacity approaches the center of the pad, allowing grooves models to be used in applications requiring less load and weight.

Nomenclature

Symbol	Description	Unit
B	Pad width	m
C, C_1, C_2	Integration constants	---
F	Friction force	N
H	Film thickness	m
h_i	Film thickness, leading edge	m
h_o	Film thickness, trailing edge	m
h_m	Maximum height when dp/dx = 0	m
K	Film ratio h_i / h_o	---
L	Pad length	m
P	Pressure	N/m^2
Q	Lubricant flow rate	m^3/s
T	Temperature	C°
u, U, V	Sliding velocity	m/s
W	Load carrying capacity	N
H	Dynamic viscosity	Kg/m. s
τ	Shear stress	N/m^2

Author Contributions

All authors contributed equally to this work.

Data Availability Statement

The data that support the findings of this study are available on request from the corresponding author.

Conflicts of Interest

The authors declare that there is no conflict of interest.

References

[1] G.W. Stachowiak, How tribology has been helping us to advance and to survive, Friction, 5 (2017) 233–247. https://doi.org/10.1007/s40544-017-0173-7

[2] A. Arslan et al., Surface Texture Manufacturing Techniques and Tribological Effect of Surface Texturing on Cutting Tool Performance: A Review, Crit. Rev. Solid State Mater. Sci., 41 (2016) 447–481. https://doi.org/10.1080/10408436.2016.1186597

[3] I. Etsion, State of the art in laser surface texturing, J. Tribol., 127 (2005) 248–253. https://doi.org/10.1115/1.1828070

[4] A. Erdemir, Review of engineered tribological interfaces for improved boundary lubrication, Tribol. Int., 38 (2005) 249–256. https://doi.org/10.1016/j.triboint.2004.08.008

[5] T. Shimizu, T. Kakegawa, and M. Yang, Micro-texturing of DLC thin film coatings and its tribological performance under dry sliding friction for microforming operation, Procedia. Eng., 81 (2014) 1884–1889. https://doi.org/10.1016/j.proeng.2014.10.251

[6] B. Bhushan, Adhesion and stiction: Mechanisms, measurement techniques, and methods for reduction, J. Vac. Sci. Technol. B Microelectron. Nanom. Struct., 21 (2003) 2262. https://doi.org/10.1116/1.1627336

[7] H. Yu, X. Wang, and F. Zhou, Geometric shape effects of surface texture on the generation of hydrodynamic pressure between conformal contacting surfaces, Tribol. Lett., 37 (2010) 123–130. https://doi.org/10.1007/s11249-009-9497-4

[8] I. Etsion, Improving tribological performance of mechanical components by laser surface texturing, Tribol. Lett., 17 (2004) 733–737. https://doi.org/10.1007/s11249-004-8081-1

[9] K. Yagi, H. Sato, and J. Sugimura, On the magnitude of load-carrying capacity of textured surfaces in hydrodynamic lubrication, Tribol. Online., 10 (2015) 232–245. https://doi.org/10.2474/trol.10.232

[10] Y. Wang, Y. Liu, Z. Wang, and Y. Wang, Surface roughness characteristics effects on fluid load capability of tilt pad thrust bearings with water lubrication, Friction, 5 (2017) 392–401. https://doi.org/10.1007/s40544-017-0153-y

[11] D. Gropper, T. J. Harvey, and L. Wang, Numerical analysis and optimization of surface textures for a tilting pad thrust bearing, Tribol. Int., 124 (2018) 134–144. https://doi.org/10.1016/j.triboint.2018.03.034

[12] Zhang, Xiaohan ,An Analysis of Surface Roughness and its Influence on a Thrust Bearing, J. Phys. Ther. Sci., 9 (2018) 1–11. https://doi.org/10.1016/j.humov.2018.08.006

[13] K. Maharshi, T. Mukhopadhyay, B. Roy, L. Roy, and S. Dey, Stochastic dynamic behaviour of hydrodynamic journal bearings including the effect of surface roughness, Int. J. Mech. Sci., 142–143 (2018) 370–383. https://doi.org/10.1016/j.ijmecsci.2018.04.012

[14] T. Dimond, A. Younan, and P. Allaire, A review of tilting pad bearing theory, Int. J. Rotating. Mach., 2011 (2011). https://doi.org/10.1155/2011/908469

[15] Kingsbury Inc., A general guide to the principles, operation and troubleshooting of hydrodynamic bearings, 2019.

[16] C. Gibert et al., Damping coefficient estimation of a squeeze-film damper operating in a dual shaft test rig To cite this version : HAL Id : hal-02456147 Damping coefficient estimation of a squeeze-film damper operating in a dual shaft test rig, Mécanique Industries, 11 (2010) 297 – 308. https://doi.org/10.1051/meca/2010067

[17] Z. Liming, L. Yongyao, W. Zhengwei, L. Xin, and X. Yexiang, A review on the large tilting pad thrust bearings in the hydropower units, Renew. Sustain. Energy. Rev., 69 (2017) 1182–1198. https://doi.org/10.1016/j.rser.2016.09.140

[18] G. Stachowiak ,A. Batchelor, Engineering Tribology 4th Edition, Butterworth Heinemann, 2013.

[19] J. Halling, Principles of Tribology , London and Basingstoke, 233, 235, 239, 242,1978.

[20] George H.F., Qureshi F. Newton's Law of Viscosity, Newtonian and Non-Newtonian Fluids. In: Wang Q.J., Chung YW. (eds) Encyclopedia of Tribology. Springer, Boston, MA,2013. https://doi.org/10.1007/978-0-387-92897-5_143

[21] Muhannad M. Mrah Studying The Tribological Characteristics Of Synthetic Oils Using Manufactured Inclined Bearing. Thesis, University of Technology, Iraq, 2022.

[22] D. Gropper, L. Wang, and T. J. Harvey, Hydrodynamic lubrication of textured surfaces: A review of modeling techniques and key findings, Tribol. Int., 94 (2019) 509–529. https://doi.org/10.1016/j.triboint.2015.10.009

[23] Yasir Akram Abd Al - Rida, Study the Influence of the Triangular Slots on the Lubrication Characteristics in the Inclined Slider Bearing, Master thesis, University of Technology, Department of Mechanical Engineering, 2011.

[24] E-radionica.com, Pressure Sensor MPS20N0040D-S_datasheet, pp. 13, [Online]. Available: https://datasheet4u.com/datasheet-pdf/ETC/MPS20N0040D-S/pdf.php?id=996460.